Environmental Science & Technology

pubs.acs.org/est

Article

Using Mercury Stable Isotopes to Quantify Bidirectional Water−Atmosphere Hg(0) Exchange Fluxes and Explore Controlling Factors

Hui Zhang, Xuewu Fu,* Xian Wu, Qianwen Deng, Kaihui Tang, Leiming Zhang, Jonas Sommar, Guangyi Sun, and Xinbin Feng

Cite This: *Environ. Sci. Technol.* 2023, 57, 10673−10685

Read Online

ACCESS | Metrics & More | Article Recommendations | Supporting Information

ABSTRACT: In this study, exchange fluxes and Hg isotope fractionation during water−atmosphere Hg(0) exchange were investigated at three lakes in China. Water−atmosphere exchange was overall characterized by net Hg(0) emissions, with lake-specific mean exchange fluxes ranging from 0.9 to 1.8 ng m^{-2} h^{-1}, which produced negative δ^{202}Hg (mean: −1.61 to −0.03‰) and Δ^{199}Hg (−0.34 to −0.16‰) values. Emission-controlled experiments conducted using Hg−free air over the water surface at Hongfeng lake (HFL) showed negative δ^{202}Hg and Δ^{199}Hg in Hg(0) emitted from water, and similar values were observed between daytime (mean δ^{202}Hg: −0.95‰, Δ^{199}Hg: −0.25‰) and nighttime (δ^{202}Hg: −1.00‰, Δ^{199}Hg: −0.26‰). Results of the Hg isotope suggest that Hg(0) emission from water is mainly controlled by photochemical Hg(0) production in water. Deposition-controlled experiments at HFL showed that heavier Hg(0) isotopes (mean ε^{202}Hg: −0.38‰) preferentially deposited to water, likely indicating an important role of aqueous Hg(0) oxidation played during the deposition process. A Δ^{200}Hg mixing model showed that lake-specific mean emission fluxes from water surfaces were 2.1−4.1 ng m^{-2} h^{-1} and deposition fluxes to water surfaces were 1.2−2.3 ng m^{-2} h^{-1} at the three lakes. Results from the this study indicate that atmospheric Hg(0) deposition to water surfaces indeed plays an important role in Hg cycling between atmosphere and water bodies.

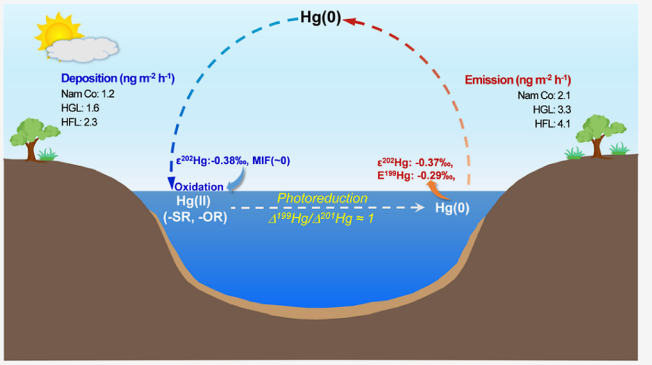

KEYWORDS: *water, −, atmosphere Hg(0) exchange, lakes, stable Hg isotope, MDF, MIF, emission, deposition*

1. INTRODUCTION

Exchange of gaseous elemental mercury (Hg(0)) between water and atmosphere plays a pivotal role in mercury biogeochemical cycling. The current exchange flux estimates are however associated with high uncertainties, and a better constraint is crucial for assessing mercury sources and sinks and associated atmospheric and biogeochemical cycling.[1] The surface layer of sea and fresh water bodies is usually in a state of supersaturation with respect to dissolved Hg(0) (DGM) as shown by extensive surveys using automatic continuous equilibrium systems.[2] Despite the fact that concentration gradients of Hg(0) between water and air are in favor of emissions, several studies report intermittent periods of net Hg(0) uptake in the flux dynamics possibly driven by high primary production (e.g. algal blooms).[1,3] Generally, net atmosphere-surface exchange of Hg(0) is a result of simultaneously occurring emissive and depositional flux vectors.[4] Atmospheric Hg(0) deposited to surface water can increase the Hg(II) pool in aquatic systems, which can subsequently convert to neurotoxic methylmercury (MeHg) that bioaccumulates in food webs.[5] In contrast, reduction of Hg(II) to Hg(0) followed by evasion to the atmosphere increases the amount of Hg actively cycling between environmental reservoirs.[6,7]

Photochemical and biotic/abiotic dark reduction are the main mechanisms causing surface water supersaturation of DGM and consequentially promoting Hg(0) emissions from water.[6,8−10] Although it has been suggested that photo-driven reduction is optimally significantly faster than thermal abiotic/biotic reduction in surface water,[8,11,12] its relative contributions currently lack a precise quantification. Furthermore, there is paucity of knowledge of the specific mechanisms that lead to prevailing Hg(0) deposition to natural waters. Incubation experiments suggest that Hg(0) oxidation rates in marine waters are fast,[11,12] while counterbalancing abiotic dark

Received: February 15, 2023
Revised: June 16, 2023
Accepted: June 16, 2023
Published: June 28, 2023

reaction and photo-induced processes are more prominent in a fresh water ligation environment.[13,14] Current models operate with Hg(0) flux partitioning into emission and deposition,[15,16] although there are still no reports of in situ methods that can do this partitioning and therefore serve as a reference for performance testing and validation. A proven approach to achieve flux partitioning is based on combining measurements of mass fluxes with sampling of stable isotopes for the specific gas of interest.

Stable Hg isotope techniques have been applied to estimate the co-occurring Hg(0) emission and deposition fluxes at the soil−atmosphere interface and quantify the atmospheric Hg deposition pathways to seawater.[17,18] Fractionation of Hg isotopes during water−atmosphere Hg(0) exchange processes could provide insights into the redox transformation and cycling of Hg in aquatic systems. Previous experimental studies revealed that all biotic and abiotic reactions can produce significant Hg mass-dependent fractionation (MDF, reported as δ^{202}Hg),[13,19−23] whereas large mass-independent fractionation (MIF) of odd-Hg isotopes (odd-MIF) (reported as Δ^{199}Hg and Δ^{201}Hg) are dominantly observed in photo-induced reactions.[13,21,24−27] The mechanism of odd-MIF is mainly attributed to the magnetic isotope effect (MIE) with the Δ^{199}Hg/Δ^{201}Hg slope of 1.0,[21, 27] but small odd-MIF can also be caused by the nuclear volume effect (NVE) with the Δ^{199}Hg/Δ^{201}Hg slope of 1.6.[13,26] In addition, MIE can assume both positive and negative values,[28] while NVE exhibits an opposite sign to MDF and increase in magnitude as MDF increases.[29] It has been experimentally demonstrated that (−)MIE and (+)MIE mainly resulted from photoreduction of Hg(II)-bonded S-containing and surfurless ligands, respectively.[30] Furthermore, the microbial reduction and Hg(0) volatilization and diffusion do not significantly affect odd-MIF.[22,31,32] More unusual, even-Hg MIF (determined as Δ^{200}Hg and Δ^{204}Hg) has been observed mainly in atmospheric samples and speculated to have resulted from dissociative processes of molecular Hg species at high altitudes.[33−35] Thus, even-MIF has been recognized as a conservative tracer to distinguish deposition pathways of atmospheric Hg species into aquatic systems.[18]

Globally, Hg(0) emission from natural waters is considered as one of the largest sources of atmospheric Hg(0),[15,16] and therefore has a potential to affect the isotopic composition of atmospheric Hg(0) and water Hg pools. Although fresh water ecosystems (including lakes, reservoirs, rivers, wetlands, and periodically flooded paddy fields) only represent 3.2% of the Earth's total water area, Hg(0) exchange between these inland water bodies and atmosphere is of importance for better understanding the biogeochemical cycling of Hg in aquatic ecosystems.[36] Knowledge of Hg isotope fractionation and bidirectional Hg(0) fluxes during water−atmosphere exchange is limited for both fresh and sea water, and the study over fresh water, to some extent, may have implications for understanding and interpretation of the sources and stable isotope signatures in sea water.[23] Previously, Hg isotopic fractionation during soil/foliage−atmosphere Hg(0) exchange has been investigated.[37−40] Mercury isotopic fractionation during chemical conversion of Hg in water has also been investigated extensively;[13,21,27,41] however, results from these studies are insufficient to make reliable predictions about the isotopic composition of DGM in water and its efflux to the atmosphere. Hg(0) emission from water is predicted to show negative δ^{202}Hg and positive Δ^{199}Hg values by a global Hg isotopic box model,[42,43] which has yet to be validated by in situ measurements.

In this study, fractionation of Hg isotopes and underlying mechanisms during water−atmosphere Hg(0) exchange were investigated at three lakes in China using a dynamic flux chamber (DFC) method. During the experiments, ambient air (gas exchange), zero Hg(0) air (emission-controlled), and spiked Hg(0) air (deposition-controlled) were separately supplied to the DFC inlet. Measuring background fluxes requires quantifying small concentration differences. The intrusive DFC method amplifies the concentration differences and enables relatively short isotope measurement times. The objectives of this study are to (1) characterize the isotopic compositions of exchanged Hg(0) between water and atmosphere, (2) quantify the individual Hg(0) emission and deposition fluxes, and (3) discern the controlling factors and mechanisms of Hg isotope fractionation during bidirectional water−atmosphere Hg(0) exchange.

2. EXPERIMENTAL METHOD AND MATERIALS

2.1. Sites' Descriptions. Three lakes in China with distinctly different characteristics were selected for investigation. Hongfeng lake (HFL) (26°26′ N, 106°26′ E, 1150 m elevation) is a typical and the largest karst lake in the Yunnan-Guizhou plateau area of southwest China. Huguangyan maar lake (HGL) (21°09′ N, 110°17′ E, 57 m elevation) is one of the well-preserved maars (broad, low-relief crater lakes) in the world and located in the tropical zone of South China. Lake Nam Co (Nam Co) (30°30′ N, 90°16′ E, 4718 m elevation) is the largest saltwater lake and the one at the highest elevation in the Tibetan Plateau (Figure S2). HFL is moderately polluted, whereas HGL and Nam Co are pristine lakes. Major input pathways of Hg are atmospheric deposition and riverine loading to HFL, atmospheric deposition to HGL, and atmospheric deposition and glacier meltwater to Nam Co. Geographical, hydrological, meteorological, and water quality data were collected at the three lakes and are presented in the Supporting Information (Text S1, Tables S1 and S3).

2.2. Measurement of Hg(0) Fluxes and Sampling and Processing of Hg(0) Isotope Samples. The Hg(0) exchange flux between water and atmosphere at the three lakes was measured using a DFC (semi-cylinder, ø 25 × 35cm) coupled with an automated Tekran 2537B Hg analyzer (Figure S3).[44] Hg(0) vapor in the DFC inlet and outlet was collected using chlorine-impregnated activated carbon (CLC, 500 mg) traps at a flow rate of 3.0−5.0 L min^{-1} for the subsequent measurement of Hg isotopes.[45] The experiment setup of Hg(0) collection is similar to that reported in previous studies[38,40] and is also documented in Text S2 and Figure S3. All the CLC traps were sealed with Teflon stoppers and three successive polyethylene bags after the completion of sampling and stored in darkness at room temperature until subsequent analysis of the Hg concentration and isotopic composition.

The Hg(0) collected on CLC traps was preconcentrated into 5 mL of 40% reverse aqua regia acid-trapping solution (v/v, 2HNO_3:1HCl) using a thermally desorbed method.[46] After the thermal combustion, the trapping solutions were kept in a 20 mL brown screw neck borosilicate glass bottle and stored in a refrigerator at 3 ± 1 °C before Hg concentration and isotopic analysis. Hg concentrations in trapping solutions were determined using a standard purge and trap method with chloride ($SnCl_2$) reduction following the USEPA method 1631.[47]

https://doi.org/10.1021/acs.est.3c01273
Environ. Sci. Technol. 2023, 57, 10673−10685

Table 1. Summary of Surface Water DHg Concentration, DFC Inlet and Outlet Hg(0) Concentration, Hg(0) Fluxes of Exchange, Disposition and Emission, Hg Isotope Signatures of DHg, DFC Inlet and Outlet Hg(0), and Exchange Hg(0) in This Study[a]

		surface water DHg							
			concn (ng L^{-1})		δ^{202}Hg (‰)		Δ^{199}Hg (‰)		Δ^{200}Hg (‰)	
lakes ID	sampling season	n	mean	1σ	mean	1σ	mean	1σ	mean	1σ
HFL	winter	6	1.65	0.33	−0.81	0.22	0.15	0.07	0.09	0.04
	spring	6	2.33	0.32	−1.31	0.48	0.34	0.13	0.07	0.03
	summer	6	2.18	0.31	−0.67	0.19	0.13	0.08	0.04	0.03
HGL	autumn	3	3.50	0.16	−0.39	0.14	0.20	0.04	0.06	0.03
Nam Co	autumn	2	0.61	0.00	2.24	0.10	0.36	0.03	0.04	0.03

		DFC inlet Hg(0)								DFC outlet Hg(0)							
		concn (ng m^{-3})		δ^{202}Hg (‰)		Δ^{199}Hg (‰)		Δ^{200}Hg (‰)		concn (ng m^{-3})		δ^{202}Hg (‰)		Δ^{199}Hg (‰)		Δ^{200}Hg (‰)	
lakes ID	sampling season	mean	1σ	mean	1σ	mean	1σ	mean	1σ	mean	1σ	mean	1σ	mean	1σ	mean	1σ
HFL	winter	6.34	2.00	−0.58	0.36	0.03	0.04	−0.01	0.03	6.75	1.96	−0.65	0.35	−0.03	0.07	0.00	0.04
	spring	4.02	0.65	−0.37	0.09	−0.03	0.05	−0.02	0.02	5.08	0.73	−0.57	0.15	−0.07	0.08	0.02	0.00
	summer	3.12	1.05	−0.45	0.19	−0.17	0.06	−0.04	0.02	4.14	1.27	−0.75	0.25	−0.20	0.05	−0.01	0.03
HGL	autumn	1.27	0.57	0.04	0.27	−0.19	0.07	−0.04	0.02	2.06	0.56	0.03	0.26	−0.16	0.07	0.02	0.02
Nam Co	autumn	1.27	0.26	0.49	0.25	−0.10	0.11	−0.02	0.04	2.19	0.49	−0.31	0.30	−0.21	0.05	0.00	0.03

		net and calculated bidirectional Hg(0) flux				exchange Hg(0) isotopes						
			δ^{202}Hg (‰)	Δ^{199}Hg (‰)	Δ^{200}Hg (‰)		δ^{202}Hg (‰)		Δ^{199}Hg (‰)		Δ^{200}Hg (‰)	
lakes ID	sampling season	n	mean	mean	mean	n	range	mean	range	mean	range	mean
HFL	winter	5	1.1	3.7	4.8							
	spring	6	2.0	2.2	4.3	5	−2.14 to −0.66	−1.16	−0.59 to −0.01	−0.28	0.07 to 0.15	0.11
	summer	9	2.1	2.7	4.7	7	−3.16 to −0.98	−1.94	−0.34 to −0.09	−0.24	0.05 to 0.12	0.07
HGL	autumn	6	1.8	5.0	6.8	5	−0.35 to 0.19	−0.03	−0.33 to −0.08	−0.16	−0.16 to 0.18	0.07
Nam Co	autumn	5	0.9	0.9	1.9	6	−2.41 to 0.27	−1.29	−0.60 to −0.05	−0.34	0.03 to 0.09	0.06

[a]Note: only CMF ≥ 0.15 of exchange Hg(0) isotopes are included in the table as discussed in the text.

https://doi.org/10.1021/acs.est.3c01273
Environ. Sci. Technol. 2023, 57, 10673−10685

Water−atmosphere Hg(0) exchange flux was quantified by measuring the difference in Hg(0) concentration of the DFC inlet and outlet. Hg(0) concentrations in the DFC inlet and outlet were calculated by dividing the total mass of Hg(0) collected (ng) by the total cumulative sampling air volume (m^3). The Hg(0) exchange flux was calculated by eq 1[38]

$$F = \frac{(C_{out} - C_{in})Q}{A} = \frac{(M_{out}/V_{out} - M_{in}/V_{in})Q}{A} \quad (1)$$

where F is the Hg(0) exchange flux in ng m^{-2} h^{-1}; C_{out} and C_{in} are the Hg concentrations of the DFC outlet and inlet air in ng m^{-3}, respectively; Q is the total flushing flow rate through the DFC in m^3 h^{-1}; A is the surface area of water in DFC in m^2 (0.0875 m^2); M_{out} and M_{in} are the mass of Hg (ng) recovered from CLC traps at the DFC outlet and inlet, respectively; and V_{out} and V_{in} are the total gas volume (m^3) in the DFC outlet and inlet air, respectively.

2.3. Measurement of Hg Isotopes in Hg(0) Emission- and Deposition-Controlled Experiments. Emission- and deposition-controlled experiments were performed at HFL to investigate the Hg isotope fractionation during Hg(0) emission from water and atmospheric Hg(0) deposition to water, respectively. The emission-controlled experiments were accomplished by using Hg-free air at the DFC inlet, which aimed to eliminate Hg(0) deposition and only collect Hg(0) emissions from water. The experimental setup of emission-controlled experiments was prepared similarly to that of soil−atmosphere Hg(0) exchange under Hg-free air exposure,[17] as detailed in Text S2 and Figure S4. Both daytime and nighttime samples were collected by CLC traps to investigate the diurnal variations in Hg(0) emission flux and isotope fractionation (Table S4).

For deposition-controlled experiments, Hg(0) vapor with known Hg mass and isotopic compositions was injected into the DFC inlet using a microliter syringe (Hamilton, USA) in the presence of Hg-free air, aiming to investigate the Hg(0) isotope fractionation during atmospheric Hg(0) deposition process. The inlet Hg(0) concentrations under deposition-controlled experiments (mean ± 1σ: 76.7 ± 7.4 ng m^{-3}, n = 6, Figure S4 and Table S4) were significantly higher than those in ambient air (Table 1) to minimize the effects of Hg(0) emission, which in turn primarily reflect the Hg isotope fractionation during Hg(0) deposition to water. During the experiments, a fraction of Hg(0) in the chamber deposited to water, and the residual Hg(0) was then collected by CLC traps to represent the Hg(0) modified by the deposition process.

2.4. Hg Isotope Analysis. The Hg isotope ratios were measured by MC-ICPMS (Nu II, Instruments, U.K.) at the State key Laboratory of Environmental Geochemistry, CAS (Guiyang, China), following the previous studies.[48,49] MDF is expressed using delta notation [δ, reported in permil (‰)] and calculated relative to the reference NIST 3133 standard as follows[50]

$$\delta^{xxx}\mathrm{Hg}\ (‰) = [((^{xxx}\mathrm{Hg}/^{198}\mathrm{Hg})_{Sample} / (^{xxx}\mathrm{Hg}/^{198}\mathrm{Hg})_{SRM3133}) - 1] \times 10^3 \quad (2)$$

where xxx is the mass number of Hg isotopes (199, 200, 201, 202, and 204). The MIF is expressed using the capital delta notation (Δ) and calculated as

$$\Delta^{xxx}\mathrm{Hg}\ (‰) = \delta^{xxx}\mathrm{Hg} - \beta^{xxx}\delta^{202}\mathrm{Hg} \quad (3)$$

where β^{xxx} is the scaling factor of the theoretical mass-dependent law and has values of 0.2520, 0.5024, 0.7520, and 1.493 for ^{199}Hg, ^{200}Hg, ^{201}Hg, and ^{204}Hg, respectively.[50] The analytical uncertainty (±2σ) of isotopic composition was assessed by repeatedly measuring standard reference RM 8610 (UM-Almaden), BCR 482 (lichen CRM), and SRM 1947 (Fish) during Hg isotope measurement. In this study, the 2σ of Hg isotopic compositions is the larger 2σ value of either the repeated analysis of the Hg(0) sample or the procedural RM 8610. (Table S2).

2.5. Hg(0) Isotopic Compositions and Emission and Deposition Fluxes during Water−Atmosphere Exchange. An isotopic binary mixing model was applied to the measurement data to determine MDF_{ex} ($\delta^{202}Hg_{ex}$) and MIF_{ex} ($\Delta^{199}Hg_{ex}$, $\Delta^{200}Hg_{ex}$, and $\Delta^{201}Hg_{ex}$) signatures for water−atmosphere Hg(0) exchange. The exchange of Hg(0) isotopic compositions were calculated as

$$\delta^{202}\mathrm{Hg}_{ex}(‰) = \frac{\delta^{202}\mathrm{Hg}_{out}C_{out} - \delta^{202}\mathrm{Hg}_{in}C_{in}}{C_{out} - C_{in}} \quad (4)$$

$$\Delta^{xxx}\mathrm{Hg}_{ex}(‰) = \frac{\Delta^{xxx}\mathrm{Hg}_{out}C_{out} - \Delta^{xxx}\mathrm{Hg}_{in}C_{in}}{C_{out} - C_{in}} \quad (5)$$

where $\delta^{202}Hg_{in}$ and $\delta^{202}Hg_{out}$ represent MDF and $\Delta^{xxx}Hg_{in}$ and $\Delta^{xxx}Hg_{out}$ represent the MIF isotopic signatures in the DFC inlet and outlet air, respectively. The calculation procedure follows the method described in a previous study.[38] Given that the Hg(0) emission and deposition occur simultaneously in the water−atmosphere exchange, this procedure allows for calculating the conclusive MDF_{ex} and MIF_{ex} signatures. Briefly, the concentration modification factor (CMF) was defined as the ratio of $(C_{out} - C_{in})/C_{out}$, aiming to separate the Hg(0) flux with significant emission (CMF > 0.15) and deposition (CMF < −0.15).[38]

A Δ^{200}Hg isotopic mass balance model was applied to quantify the contribution of the individual flux components to the total Hg(0) flux during the water−atmosphere Hg(0) exchange process. The Hg(0) flux of emission from or deposition to water was determined by the following equation

$$F_{Emis} = \frac{C_{inlet}V_{out}(\Delta^{200}\mathrm{Hg}_{out} - \Delta^{200}\mathrm{Hg}_{in})}{Ah(\Delta^{200}\mathrm{Hg}_{water} - \Delta^{200}\mathrm{Hg}_{out})} \quad (6)$$

$$F_{Dep} = F_{Emis} - F \quad (7)$$

where F_{Emis} and F_{Dep} represent the Hg(0) emission flux from and deposition flux to water (ng m^2 h^{-1}), respectively, and h is the sampling duration. $\Delta^{200}Hg_{water}$ is the DHg isotopic compositions in surface water, which was collected by the CLC traps method (Text S3).[46] DHg represents the sum of dissolved Hg(0) and Hg(II). The detailed information of the calculation method can be found in Text S4.

Based on the Hg isotopic mass balance model, the MIF of Hg(0) emissions ($\Delta^{xxx}Hg_{Emis}$, with xxx being 199 or 200) during water−atmosphere exchange was calculated as follows

$$\Delta^{xxx}\mathrm{Hg}_{Emis} = [\Delta^{xxx}\mathrm{Hg}_{outlet}C_{outlet} V_{outlet}(F_{Emis}Ah + C_{inlet}V_{outlet}) - \Delta^{xxx}\mathrm{Hg}_{inlet}C_{in} V_{outlet}(C_{in}V_{outlet} + FAh)]/[(F_{Emis}Ah(C_{in} \times V + FAh))] \quad (8)$$

https://doi.org/10.1021/acs.est.3c01273
Environ. Sci. Technol. 2023, 57, 10673−10685

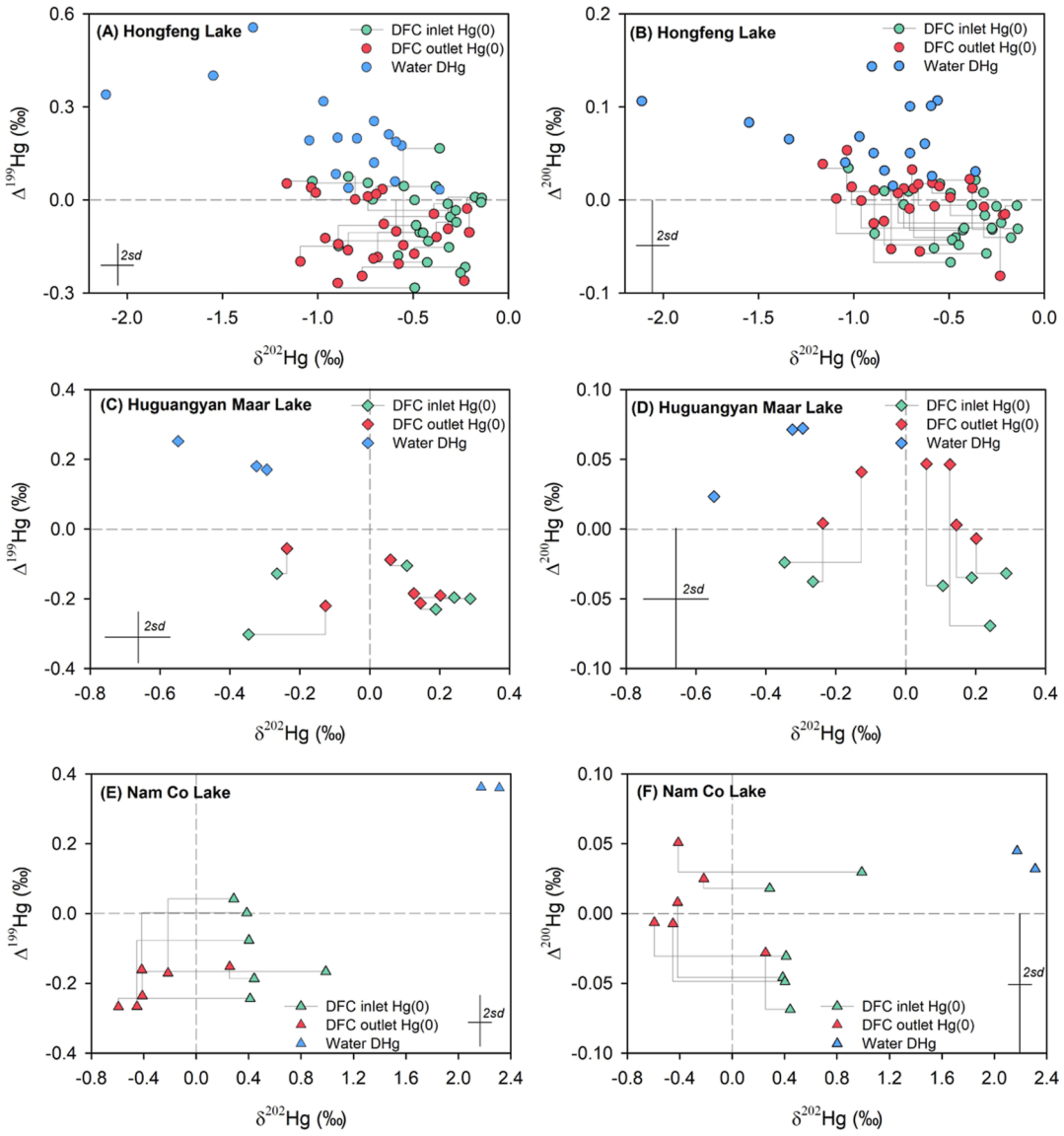

Figure 1. MDF (δ^{202}Hg) and MIF (Δ^{199}Hg and Δ^{200}Hg) isotope signatures of DFC inlet, outlet Hg(0), and water DHg in HFL (A,B), HGL (C,D), and Nam Co lake (E,F). The gray lines are used to connect isotopic compositions of Hg(0) at the inlet and outlet of the flux chamber in each of the lakes.

where F_{Emis} is the Hg(0) emission flux from water (ng m^{-2} h^{-1}). A detailed description of this method can be found in Text S5.

2.6. Quality Assurance and Control. The chamber blank was determined in the field by using an ultraclean quartz plate on the chamber bottom, which showed negligible blanks (0.10 ± 0.12 ng m^{-2} h^{-1}, 1σ, n = 15). Full procedural blanks with 500 mg CLC traps were thermally desorbed and preconcentrated into 5 mL of acid-trapping solution. The mean procedural blank was 0.056 ± 0.024 ng mL^{-1} (1σ, n = 6), which is negligible (<6%) compared to the Hg concentrations in the final trapping solution. The DFC inlet and outlet of Hg(0) concentrations were continuously measured using CLC trap collection in parallel to the automated Tekran 2537B Hg analyzer at HFL and Nam Co. Nearly identical Hg(0) concentrations were observed between those two methods (Figure S5). More importantly, the DFC technique does not significantly introduce Hg isotope bias effects,[38] indicating that this method can accurately measure the isotopic compositions during the water−atmosphere Hg(0) exchange process.

The standard references of RM 8610, BCR 482, and SRM 1947 were measured during Hg isotope analysis to obtain the analytical uncertainties of instrumental procedures and laboratory preconcentration. The measured Hg isotopic signatures of the three standards were consistent with recommended values (Table S2).[51,52]

3. RESULTS AND DISCUSSION

3.1. Concentrations and Isotopic Compositions of Water-Dissolved Hg and Atmospheric Hg(0). Average DHg concentrations at the HFL (n = 18), HGL (n = 3), and Nam Co (n = 2) were 2.05 ± 0.42 (1σ), 3.50 ± 0.16, and 0.61 ng L^{-1}, respectively (Table S3). These values were similar to the DHg concentrations (0.28−1.19 ng L^{-1}) observed for lakes in Canada[53] but slightly higher than the DHg concentrations in seawater (0.30−0.78 ng L^{-1}).[18] Mean δ^{202}Hg values of DHg in surface water at HFL, HGL, and Nam Co were −0.93 ±

https://doi.org/10.1021/acs.est.3c01273
Environ. Sci. Technol. 2023, 57, 10673−10685

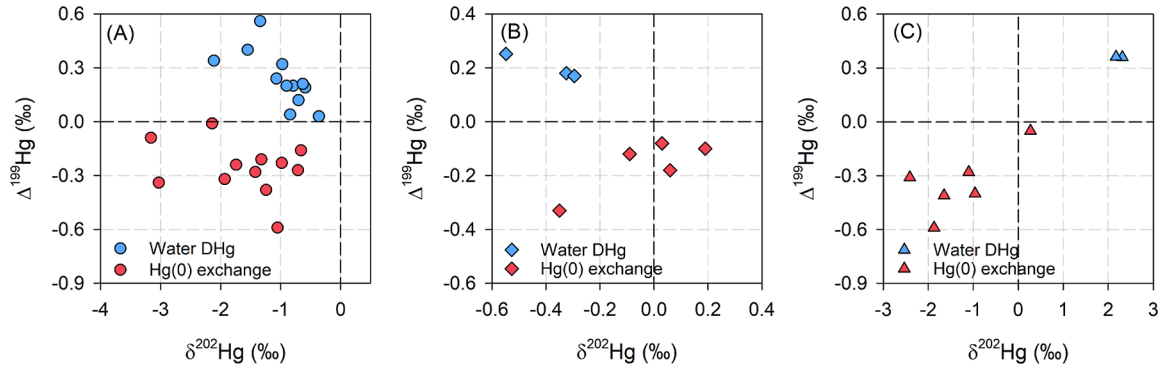

Figure 2. Hg isotopic compositions (Δ^{199}Hg versus δ^{202}Hg) of exchange Hg(0) between water and atmosphere. (A) HFL, (B) HGL, and (C) Nam Co.

0.41‰ (n = 18), −0.39 ± 0.14‰ (n = 3), and 2.24 ± 0.10‰ (n = 2), respectively (Figure 1, Tables 1 and S3). DHg samples at the three lakes show positive Δ^{199}Hg (mean ± 1σ: HFL = 0.21 ± 0.13‰, HGL = 0.20 ± 0.04‰, Nam Co = 0.36 ± 0.04‰) and slightly positive Δ^{200}Hg signatures (mean ± 1σ: HFL = 0.07 ± 0.03‰, HGL = 0.06 ± 0.03‰, Nam Co = 0.04 ± 0.03‰). The DHg isotopic compositions of HFL and HGL are similar to those reported for DHg at lakes in Ontario, Canada[53] and THg in seawater.[18]

Ambient air DFC inlet Hg(0) concentrations at HGL (mean ± 1σ: 1.27 ± 0.57 ng m^{-3}, n = 6) and Nam Co (mean ± 1σ: 1.27 ± 0.26 ng m^{-3}, n = 6) were similar to the background values (<1.5 ng m^{-3}),[54] but those at HFL (mean ± 1σ: 4.57 ± 2.02 ng m^{-3}, n = 26) were about four times higher (Tables 1 and S6). Air at HFL was affected by anthropogenic emissions while at HGL and Nam Co, it was essentially pristine. Our observations of DFC inlet Hg(0) enriched with lighter isotopes at HFL (mean δ^{202}Hg: −0.48‰) and heavier isotopes at HGL (mean δ^{202}Hg: 0.04‰) and Nam Co (mean δ^{202}Hg: 0.49‰) are in agreement with literature reported values.[55] The mean Δ^{199}Hg of the DFC inlet Hg(0) were determined to be −0.06‰ ± 0.10‰ (±1σ) for HFL, −0.19‰ ± 0.07‰ (±1σ) for HGL, and −0.10‰ ± 0.11‰ (±1σ) for Nam Co. Mean Δ^{200}Hg of inlet Hg(0) at the three lakes ranged from −0.04 to −0.02‰. The isotopic compositions of the DFC inlet ambient air Hg(0) at HFL are overall consistent with those previously observed at an adjacent urban site in Guiyang (−0.96‰ and −0.01‰ for δ^{202}Hg and Δ^{199}Hg, respectively), which was attributed to regional anthropogenic emissions.[56] The inlet Hg(0) isotopic compositions at HGL and Nam Co are overall similar to those observed at background sites.[55] There are no significant relationships between Hg fluxes and the isotopic compositions of Hg(0) in the DFC inlet at the three lakes (Figure S6), indicating that water Hg(0) emission was not a dominant factor controlling ambient air Hg(0) isotopic compositions.

Mean DFC outlet Hg(0) concentrations at the lakes (5.36, 2.06, and 2.19 ng m^{-3} at HFL, HGL, and Nam Co, respectively) were elevated compared to the supply of ambient air Hg(0). The mean δ^{202}Hg and Δ^{199}Hg values of DFC outlet Hg(0) were −0.67 ± 0.27‰ and −0.10 ± 0.10‰ (1σ, n = 26), respectively, at HFL, 0.03 ± 0.17‰ and −0.16 ± 0.07‰ (1σ, n = 6), respectively, at HGL, and −0.31 ± 0.30‰ and −0.21 ± 0.05‰ (1σ, n = 6), respectively, at Nam Co (Figure 1, Tables 1 and S6). Corresponding Δ^{200}Hg values were all near-zero (means = 0.00−0.02‰, n = 3). The isotopic shift (Δ) during water−atmosphere Hg(0) exchange was assessed by comparing the DFC inlet and outlet Hg(0) compositions (i.e., Δ = DFC outlet−inlet, Figure S7). Δ-δ^{202}Hg and Δ-Δ^{199}Hg at Nam Co were considerably negative (mean: −0.79‰ and −0.11‰, respectively), indicating a steady shift toward a lighter and an odd isotope-depleted Hg(0) vapor exchanged with the water surface. As can be seen from Figure 1, both negative and positive differences were observed in the chamber measurements at HFL and HGL. At HGL, mean Δ-δ^{202}Hg and Δ-Δ^{199}Hg values were indistinguishable from zero (−0.01‰ and 0.03‰ for Δ-δ^{202}Hg and Δ-Δ^{199}Hg, respectively). Mean Δ-δ^{202}Hg and Δ-Δ^{199}Hg values at HFL were −0.19‰ and −0.04‰, respectively, the magnitudes of which were much lower than those at Nam Co.

3.2. Water−Atmosphere Hg(0) Exchange Fluxes and Isotopic Compositions. Water−atmosphere Hg(0) exchange with prevailing net Hg(0) emissions were observed during all measurement campaigns (Tables 1 and S6), with slightly lower fluxes at Nam Co (mean ± 1σ: 1.2 ± 0.7 ng m^{-2} h^{-1}, n = 6) than HFL (mean ± 1σ: 1.5 ± 1.0 ng m^{-2} h^{-1}, n = 26) and HGL (mean ± 1σ: 1.8 ± 1.1 ng m^{-2} h^{-1}, n = 6). These fluxes were comparable to previous measurements at Wujiang River (2.4 ± 1.5 ng m^{-2} h^{-1} ng m^{-2} h^{-1}),[44] Yellow Sea (0.5 ± 1.3 ng m^{-2} h^{-1}),[57] Eastern Mediterranean (2.2 ± 1.5 ng m^{-2} h^{-1}),[58] and the Arctic Ocean (2.4 ng m^{-2} h^{-1}).[59]

Hg(0) isotopic compositions were calculated for all the flux exchange data except winter data at HFL due to diminutive net Hg(0) flux (CMF ≤ 0.15). Overall, the Hg(0) isotopic fractionation during water−atmosphere exchange at the three lakes was characterized by negative δ^{202}Hg$_{ex}$ and Δ^{199}Hg$_{ex}$ values and slightly positive Δ^{200}Hg$_{ex}$ values (Figure 2, Tables 1 and S5). Specifically, δ^{202}Hg$_{ex}$ varied from −3.16 to −0.66‰ (mean ± 1σ: −1.61 ± 0.83‰, n = 12) at HFL, from −0.35 to 0.19‰ at HGL (mean ± 1σ: −0.03 ± 0.20‰, n = 5), and from −2.41 to 0.27‰ at Nam Co (mean ± 1σ: −1.29 ± 0.93‰, n = 6); Δ^{199}Hg$_{ex}$ varied from −0.59 to −0.01‰ (mean ± 1σ: −0.26 ± 0.15‰, n = 12) at HFL, from −0.33 to −0.08‰ at HGL (mean ± 1σ: −0.16 ± 0.10‰, n = 5), and from −0.60 to −0.05‰ at Nam Co (mean ± 1σ: −0.34 ± 0.18‰, n = 6). Mean Δ^{200}Hg$_{ex}$ was slightly positive in all three lakes (ranged from 0.06 to 0.09‰) (Figure S8). The direction and magnitude of mean δ^{202}Hg$_{ex}$ signatures align well with those predicted by a global Hg isotope box model,[42] while the calculated odd-MIF signatures in this study (mean E^{199}Hg = −0.76 to −0.32‰, Section 3.5) deviate from simulated values (e.g., E^{199}Hg = 0.00−0.55‰[42,43]).

3.3. Isotope Fractionation during Hg(0) Deposition to Water. The mean Hg(0) deposition fluxes were 29.3 ± 3.8 ng

https://doi.org/10.1021/acs.est.3c01273
Environ. Sci. Technol. 2023, 57, 10673−10685

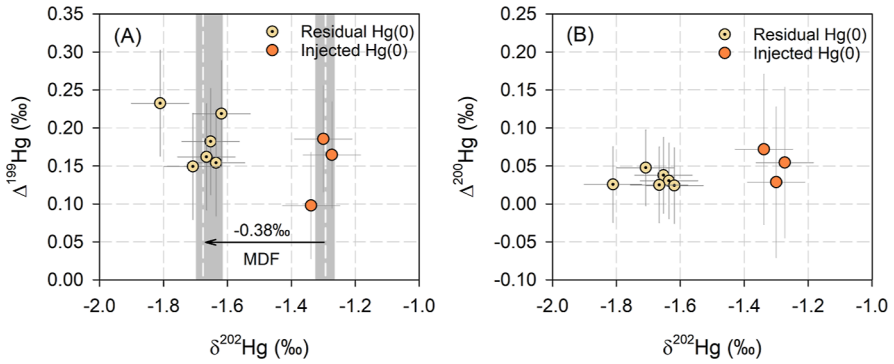

Figure 3. Fractionation of Hg isotopes during Hg(0) deposition to water. (A) Odd-MIF (Δ^{199}Hg) versus MDF (δ^{202}Hg). (B) Even-MIF (Δ^{200}Hg) versus MDF (δ^{202}Hg). The dashed line and shaded area indicate the mean and interquartile range (IQR), respectively. Error bars indicate the 2σ analytical uncertainty.

m^{-2} h^{-1} (1σ, n = 3) and 27.5 ± 14.2 ng m^{-2} h^{-1} (1σ, n = 3) during daytime and nighttime deposition-controlled experiments at HFL, respectively. The mean (±1σ) isotopic compositions of injected Hg(0) were −1.30 ± 0.03‰ for δ^{202}Hg, 0.15 ± 0.05‰ for Δ^{199}Hg, and 0.05 ± 0.02‰ for Δ^{200}Hg (Table S4). The isotopic compositions of residual Hg(0) exiting the DFC showed δ^{202}Hg values of −1.70 ± 0.10‰ (mean ± 1σ, n = 3) and −1.66 ± 0.05‰ (mean ± 1σ, n = 3), Δ^{199}Hg values of 0.19 ± 0.04‰ and 0.18 ± 0.04‰, and Δ^{200}Hg values of 0.03 ± 0.03 and 0.03 ± 0.03‰ during daytime and nighttime, respectively (Figure 3 and Table S4). There are no significant differences in deposition fluxes as well as MDF and MIF signatures between the daytime and nighttime (paired sample t-test, p = 0.20, 0.41, 0.82, and 0.67 for flux, δ^{202}Hg, Δ^{199}Hg, and Δ^{200}Hg, respectively, n = 3), implying that photochemical processes likely played a minor role in regulating the deposition fluxes and isotope fractionation of Hg(0) during atmosphere−water depositions. We observed negative MDF enrichment factors (mean $\varepsilon^{202}Hg_{Hg(0)\ residual\text{-}Hg(0)\ injected} = \delta^{202}Hg_{Hg(0)\ residual} - \delta^{202}Hg_{Hg(0)\ injected}$ = −0.38‰, Figure 3) during Hg(0) deposition to surface water, which are of the opposite sign to those for Hg(0) deposition to foliage and soils previously observed by the DFC method that show preferential enrichment of heavier isotopes in the residual Hg(0).[37−39] The deposition-controlled experiments showed negligible MIF of the odd- and even-mass Hg isotopes, with the mean MIF enrichment factors ($E^{199}Hg_{residual\ Hg(0)\text{-}injected\ Hg(0)} = \Delta^{199}Hg_{residual\ Hg(0)} - \Delta^{199}Hg_{injected\ Hg(0)}$ and $E^{200}Hg_{residual\ Hg(0)\text{-}injected\ Hg(0)} = \Delta^{200}Hg_{residual\ Hg(0)} - \Delta^{200}Hg_{injected\ Hg(0)}$) of 0.03 and −0.02‰, respectively (Figure 3).

Previous non-isotopically experimental studies suggested that Hg(0) oxidation in aquatic systems can be both non-photochemically and photochemically mediated. For example, Hg(0) oxidation can be affected by a variety of factors including environmental controls (e.g., solar radiation)[11,14] and substrate characteristics (e.g., thiol functional groups and oxidizing compounds).[10,60,61] We interpret that the observed enrichment of lighter isotopes in the air was modified by deposition process driven by aqueous phase oxidation, knowing that the oxidation process would cause enrichment of heavier isotopes in the oxidized portion.[13,62] Dark abiotic Hg(0) oxidation by humic acids and thiols has been observed to produce an enrichment of lighter isotopes in residual Hg(0) fraction ($\varepsilon^{202}Hg_{Hg(II)-Hg(0)}$ = 1.10−1.54‰), which implies a predominance of equilibrium isotope effect.[13] Besides, photo-oxidation of Hg(0) also causes an enrichment of lighter isotopes and depletion of odd isotopes in the residual Hg(0) portion, with MDF and odd-MIF enrichment factors of 3.3 and −0.35‰, respectively.[63] The deposition processes generate relatively small odd-MIF signals in our study, which should be attributed to the minor fraction of deposited Hg(0) (i.e., mean of 10%, Table S4) and the small magnitude of odd-MIF triggered by photochemical and non-photochemical Hg(0) oxidation. Figure S9 shows the Hg(0) isotopic compositions as a function of the remaining fraction of injected Hg(0).[13,63] Rayleigh fractionation models based on the MDF and odd-MIF fractionation factors obtained from dark abiotic and photochemical Hg(0) oxidations could overall accommodate our field observations; we therefore postulate that aqueous Hg(0) oxidation is an important driver of Hg(0) uptake by fresh water.

Gas-phase Hg(0) oxidation followed by Hg(II) dry deposition could also be a potential mechanism responsible for the observed isotopic fractionation during Hg(0) deposition to water. A previous laboratory study observed that gas-phase Hg(0) oxidation induced by Br atoms enriches lighter isotopes and depletes odd-isotopes in the residual Hg(0), with MDF and odd-MIF enrichment factors of 0.76−0.96 and −0.36 to −0.27‰, respectively,[64] similar to the Hg isotope fractionation during aqueous phase Hg(0) oxidation.[13,63] However, the average gas-phase Hg(0) oxidation rate in humic air in the planetary boundary layer according to the GEOS-Chem model by Shah et al. is close to 0.017 d^{-1},[65] which is 1−2 orders of magnitude lower than the values observed in natural waters (0.06−0.9 d^{-1}).[14,60,66] Therefore, we propose that the aqueous phase oxidation is the dominant process controlling the Hg(0) deposition to water, although the effect of gas-phase oxidation can be ruled out. The thin film gas exchange model seems to provide a plausible explanation for Hg(0) oxidation that occurs at the water surfaces. Since Hg(0) emission and deposition occurred simultaneously, if Hg(0) was rapidly oxidized in the thin film layers then Hg(0) deposition would be enhanced and Hg exchange should occur in both directions even if surface water is supersaturated with Hg(0) below the thin-film layer. Further studies are needed to gain a better understanding of the processes and mechanisms controlling the Hg(0) deposition to water surfaces.

3.4. Isotope Fractionation during Hg(0) Emission from Water. During the DFC experiments with supplied air free of Hg(0) at HFL, the observed effluxes were on average almost four times larger compared to the case with the

https://doi.org/10.1021/acs.est.3c01273
Environ. Sci. Technol. 2023, 57, 10673−10685

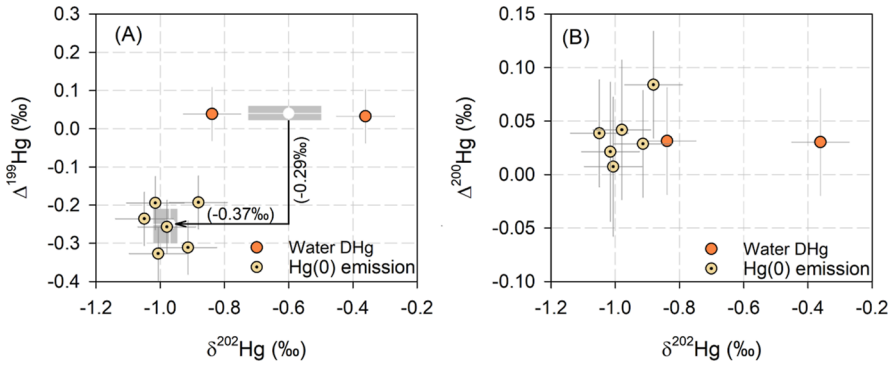

Figure 4. Fractionation of Hg isotopes during Hg(0) emission from water. (A) Odd-MIF (Δ^{199}Hg) versus MDF (δ^{202}Hg). (B) Even-MIF (Δ^{200}Hg) versus MDF (δ^{202}Hg). The shaded area and white line indicate the IQR and the mean, respectively. Error bars indicate the 2σ analytical uncertainty.

supplied ambient air [7.8 ± 2.6 ng m^{-2} h^{-1} (±1σ, n = 6, Table S4) versus 2.1 ng m^{-2} h^{-1}]. Such a marked difference implies that emission of Hg(0) from the water surface to air was substantially reduced by the smaller concentration gradient between water and air in the case of suppling ambient air, or equivalently, we could say that the emission flux was offset by co-occurring Hg(0) deposition during ambient atmosphere−water Hg(0) gas exchange. Higher daytime (mean ± 1σ: 10.1 ± 0.3 ng m^{-2} h^{-1}, n = 3) than nighttime Hg(0) emission fluxes (mean ± 1σ: 5.4 ± 0.9 ng m^{-2} h^{-1}, n = 3) were observed, and in addition, a significant positive correction between Hg(0) emission flux and solar radiation (R^2 = 0.96, p < 0.01, Figure S10) was identified, indicating that photoreduction likely plays a major role in Hg(0) emissions from water. δ^{202}Hg and Δ^{199}Hg signatures of Hg(0) emissions from water exhibited negative values during both daytime and nighttime (mean ± 1σ: δ^{202}Hg = −0.95 ± 0.09‰ and Δ^{199}Hg = −0.25 ± 0.06‰ for daytime, and δ^{202}Hg = −1.00 ± 0.05‰ and Δ^{199}Hg = −0.26 ± 0.07‰ for nighttime). The MDF enrichment factor ($\varepsilon^{202}Hg_{Hg(0)\text{-}DHg}$ = $\delta^{202}Hg_{Hg(0)}$ - $\delta^{202}Hg_{DHg}$) for Hg(0) emissions from water was −0.37 ± 0.06‰ (mean ± 1σ, n = 6); this direction was similar to Hg(0) emitted from soils (mean $\varepsilon^{202}Hg_{Hg(0)\text{-soil}}$ = −1.98‰ to −0.86‰) that enriches the lighter isotopes in the Hg(0) product.[17,40] The odd-MIF enrichment factor ($E^{199}Hg_{Hg(0)\text{-}DHg}$ = $\Delta^{199}Hg_{Hg(0)}$ − $\Delta^{199}Hg_{DHg}$) in emission-controlled experiments was −0.29 ± 0.06‰ (mean ± 1σ, n = 6, Figure 4 and Table S4), and the even-MIF enrichment factor ($E^{200}Hg_{Hg(0)\text{-}DHg}$ = $\Delta^{200}Hg_{Hg(0)}$ − $\Delta^{200}Hg_{DHg}$) during Hg(0) emissions from water exhibited values that were indistinguishable from zero (mean $E^{200}Hg_{Hg(0)\text{-}DHg}$ = 0.01 ± 0.03‰, n = 6).

3.5. Mechanisms and Controlling Factors during Water−Atmosphere Hg(0) Exchange. The effect of physicochemical properties of water on Hg redox chemistry during water−atmosphere exchange seems to be complicated, as indicated by insignificant correlation between physicochemical properties of water and flux and isotope composition of Hg(0) (Figure S11). Reduction channels that increase the Hg(0) pool in surface water and thus propel Hg effluxes to the atmosphere may include both photo-driven and dark processes. Isotopically, these processes exhibit distinctly different trajectories in terms of fractionation of the odd isotopes ^{199}Hg and ^{201}Hg. The Δ^{199}Hg/Δ^{201}Hg slope of 1.00 ± 0.08 (±1σ, Figure S12) from the regression of the odd-MIF data of the emission-controlled experiments suggests that these effluxes bear a signature typical of photo-induced MIE[21,27,30,67] with no traceable contribution from NVE-associated abiotic dark reduction.[26] Note that if both reduction processes were important for Hg(0) emissions from water, a slope that lies between 1.0 and 1.6 would be observed. Rates for photo-driven reduction are more than 1 order of magnitude higher than for dark abiotic reduction (Table S8),[8,11,12] so we expect a low contribution from the dark abiotic reduction. Microbial reduction may be a potential factor; however, this process is also expected to play a minor role in water Hg(0) emissions in the present study (more details in Text S5.2). Our stable isotope result is in good agreement with non-isotopic observations,[8,11,12] which mostly showed that Hg(0) emission from water is dominated by photochemical reduction processes. Statistical analysis showed no significant difference in odd-MIF composition between daytime and nighttime segregated efflux samples (paired sample T test, p = 0.61 for Δ^{199}Hg). We thus assume that the pool of dissolved Hg(0) formed photochemically in daylight was large enough to also maintain Hg(0) effluxes during nighttime. Based on the nighttime Hg(0) emission effluxes of 4.4−6.2 ng m^{-2} h^{-1} (means = 5.4 ng m^{-2} h^{-1}) at HFL, we roughly estimated that nocturnal Hg(0) emissions from water (a 1 m^2 surface area and 30 m deep water column) accounted for 3.7% of total DGM in the water column (Table S7), indicating that photoreduction of DGM in daytime was sufficient to maintain Hg(0) emissions at nighttime. Gustin et al.[68] proposed that light on surface soil provides energy for photochemical reduction of Hg(II) to Hg(0) to volatilization at night, a theory that supports our hypothesis above.

The calculated isotopic compositions of Hg(0) emission during water−atmosphere exchange at the three lakes exhibited negative $\Delta^{199}Hg_{Emis}$ values (eq 8, means = −0.40 to −0.12‰, n = 3). Mean values of $\Delta^{200}Hg_{Emis}$ at the three lakes ranged from 0.04−0.06‰, which are similar to the Δ^{200}Hg values of surface water DHg (Figure S13). The Δ^{199}Hg/Δ^{201}Hg slopes are 1.01, 1.00, and 1.10 at HFL, HGL, and Nam Co, respectively (Figure S14). These slopes are lower than the slope (∼1.6) associated with NVE but consistent with that of Hg(II) photoreduction due to MIE (∼1.0−1.2).[21,27,67,69] In addition, the mean odd-MIF enrichment factor ($E^{199}Hg_{Emis}$ = $\Delta^{199}Hg_{Emis}$ − $\Delta^{199}Hg_{DHg}$) exhibited negative values among the lakes (means = −0.76 to −0.32‰, n = 3), which resemble the sign but are less negative than observations from photoreduction of Hg(II) complexed with sulfurless ligands (−0.99 to −6.61‰).[21,67] Based on the observed Hg/DOC ratios presented here (mean ±1σ: HFL:

https://doi.org/10.1021/acs.est.3c01273
Environ. Sci. Technol. 2023, 57, 10673−10685

0.56 ± 0.11 ng mg^{-1}, HGL: 0.85 ± 0.08 ng mg^{-1}, and Nam Co: 0.21 ± 0.01 ng mg^{-1}), it appears that the odd-MIF enrichment factor is controlled by Hg/DOC ratios, which may explain the lower values of $E^{199}Hg_{Emis}$ than that of photoreduction of Hg(II) with high Hg/DOC ratios in laboratory experiments.[21,67] Previous studies have demonstrated that Hg preferentially bound to the S-containing functional groups in DOM at relatively low Hg/DOC ratios.[70,71] However, most Hg(0) generated by photoreduction of Hg(II) in natural water bodies stems from a sulfurless bonding environment due to high abundance of O/N ligands in natural DOM.[30,70,71] Besides, much higher Hg(II) reduction rates of sulfurless ligands than S-containing ligands in DOM were observed,[67,70,72] suggesting that cumulative Hg(II) photoreduction of sulfurless ligands may be significant on a long-time scale. Therefore, a significantly negative $E^{199}Hg_{Hg(0)\text{-}DHg}$ overall reflects a prevailing control of photoreduction of Hg(II) bound to sulfurless ligands, while a less negative value is likely attributed to the combined result of co-occurring S-containing and sulfurless ligands.

The calculated $\Delta^{199}Hg_{Emis}$ of Hg(0) emission was −0.23 ± 0.14‰ at HFL, −0.12 ± 0.10‰ at HGL, and −0.40 ± 0.25‰ at Nam Co. Interestingly, the calculated $\Delta^{199}Hg_{Emis}$ values of Hg(0) emission at HFL are consistent with that from the emission-controlled experiment (mean = −0.25‰). No significant relationships were observed between solar radiation and $E^{199}Hg_{Emis}$ of net Hg(0) emission from any of the lakes (p = 0.74). This contradicts the results of previous photochemical experiments[21,67] but is similar to those of Hg isotopic fractionation during emission-controlled experiments in both daytime and nighttime Hg(0) samples mentioned above. We therefore concluded that the odd-MIF of water emission Hg(0) during both daytime and nighttime at the three lakes is mainly caused by water Hg(II) photoreduction. Motta et al.[27] observed that the photochemical reduction of Hg(II) in the presence of cysteine with the condition of oxic pH 7 exhibited the positive $E^{199}Hg$ (0.25‰). Zheng and Hintelmann[67] proposed that the significantly negative $E^{199}Hg$ (−2.75‰) during photoreduction of Hg(II) bound to sulfurless ligands in the condition of a low Hg/DOC ratio (35 ng mg^{-1}). Therefore, based on experimentally derived fractionation factors, we roughly estimated that photoreduction of Hg(II) associated with surfurless ligands contributed 19−34%, while those associated with S-containing ligands contributed 66−81% to the total Hg(0) emissions from the surface water at the three lakes (Text S5). These percentage contributions of different types of ligands for photoreduction of Hg(II) are comparable to previously reported values generated from equilibrium models.[70] Our results indicate that the photoreduction of Hg(II) in surface water may preferentially result in relatively small (+)MIE because of the co-occurring effects of Hg binding to surfurless and S-containing ligands in surface water, which may also explain the positive $\Delta^{199}Hg$ values in water Hg(II).

Water−atmosphere exchange and atmospheric deposition [including Hg(0) and Hg(II) deposition] and Hg sedimentation are the major processes controlling the Hg cycling in aquatic systems. Hg sedimentation is not expected to induce significant odd-Hg MIF,[73] and the odd-MIF signatures of Hg in water should be therefore mainly regulated by atmospheric Hg deposition and water Hg(0) emissions. Here, we plotted the $\Delta^{199}Hg$ vs $\Delta^{200}Hg$ values of DHg measured in this and previous studies,[18,53] and we found that most $\Delta^{199}Hg$ values are scattered above the mixing line of atmospheric Hg(0) and Hg(II) deposition (Figure S15). This likely indicates that some post-deposition processes in water might also cause a positive shift of $\Delta^{199}Hg$ in water DHg. We therefore speculate whether such a positive $\Delta^{199}Hg$ shift is caused by water Hg(0) emission. Given the sedimentation fluxes and water−atmosphere Hg(0) exchange fluxes as well as the MIF signatures of Hg isotopes during water−atmospheric exchange at HFL, HGL, and Nam Co (Figure S16),[74−76] we estimated that Hg(0) emission from water would potentially yield a 0.01, 0.05, and 0.35‰ positive shift in $\Delta^{199}Hg$ of water DHg at the three lakes, respectively, using the Rayleigh equation.[43] This could well explain the measured $\Delta^{199}Hg$ shift of DHg relative to atmospheric deposition at these lakes (0.03−0.26‰) (Figure S15). The effect of Hg(0) emission on the water DHg $\Delta^{199}Hg$ is mainly controlled by the emission/sedimentation flux ratios, with a relatively higher value occurring in the pristine Nam Co where the Hg sedimentation flux is fairly low (Figure S16).

3.6. Estimate of the Hg(0) Emission and Deposition Fluxes. At present, models operate with schemes separating the deposition flux to and emission flux from the oceans, and still no in situ method has been presented that has the capacity to measure this flux partitioning and therefore act as a refs15 16,. We applied a $\Delta^{200}Hg$ mass balance model to quantify Hg(0) emission and deposition fluxes during dynamic bidirectional water−atmosphere Hg(0) exchange processes. The detailed calculations of $\Delta^{200}Hg$ mass balance can be found in Text S4. The uncertainties on the calculated F_{Emis} and F_{Dep} were estimated using a Monte Carlo approach (Text S6). Hg(0) emission and deposition fluxes at HFL (mean ± 1σ, 4.1 ± 5.0 ng m^{-2} h^{-1} and 2.3 ± 1.1 ng m^{-2} h^{-1}, respectively, Figure 5, Tables 1 and S6) were generally higher than those at HGL (mean ± 1σ, 3.3 ± 4.3 ng m^{-2} h^{-1} and 1.6 ± 1.1 ng m^{-2} h^{-1}, respectively) and Nam Co (mean ± 1σ, 2.1 ± 3.2 ng m^{-2} h^{-1} and 1.2 ± 0.4 ng m^{-2} h^{-1}). The Hg(0) deposition fluxes obtained in this study (means: 1.2−2.3 ng m^{-2} h^{-1}, n = 3) are similar to previously reported values to various terrestrial and aquatic systems by isotope approaches and modeling studies, respectively (e.g., forest: 1.0−5.5 ng m^{-2} h^{-1};[17,77,78] background soils: 4.7−14.3 ng m^{-2} h^{-1};[38] seawater: 0.3−0.5 ng m^{-2} h^{-1},[15,16] Figure S17). The finding in this and earlier studies confirm that Hg(0) deposition is a widely distributed phenomenon over various types of earth's surfaces, which

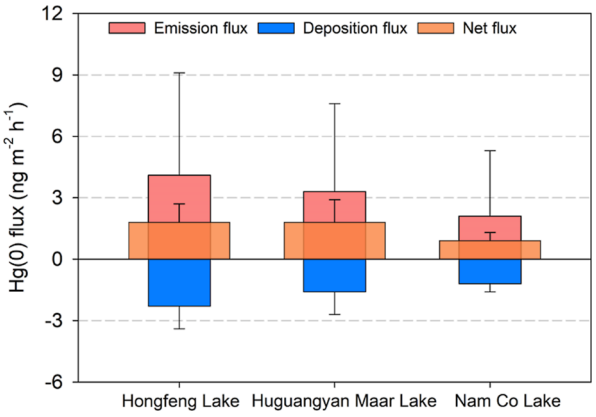

Figure 5. Hg(0) emission, deposition, and net flux at HFL, HGL and Nam Co. Error bars are 1σ analytical uncertainty of the Hg(0) flux.

https://doi.org/10.1021/acs.est.3c01273
Environ. Sci. Technol. 2023, 57, 10673−10685

would therefore play an important role in the biogeochemical cycling of Hg. Based on the estimated Hg(0) deposition fluxes, we calculated the mean Hg(0) deposition velocities of 0.02, 0.03, and 0.02 cm s^{-1} for HFL, HGL, and Nam Co, respectively.

Wet deposition is traditionally regarded as an important pathway for Hg loading to the natural water. Previous studies observed that the mean Hg wet deposition fluxes at HFL, HGL, and Nam Co were 1.44, 1.22 (in background area), and 0.21 ng m^{-2} h^{-1}, respectively.[79] These values are 1.6, 1.3, and 5.8 times lower than the Hg(0) dry deposition fluxes in the corresponding study areas (means: 1.2−2.3 ng m^{-2} h^{-1}), suggesting that Hg(0) dry deposition is a dominant source (range from 56 to 85% with a mean of 68%) of Hg in these lake ecosystems, as is the case of atmospheric Hg(0) deposition to seawater.[18]

4. ENVIRONMENTAL IMPLICATIONS

The present study observed that heavier Hg(0) isotopes are preferentially deposited to the aqueous phase ($\varepsilon^{202}Hg_{residual\text{-}injected}$ = −0.38‰), plausibly an effect of the fact that dissolved gas is readily consumed by oxidation. In turn, Hg(0) emissions from surface water, including a contribution from residual DGM, preferentially release lighter isotopes and are depleted in odd-mass-number isotopes (mean ε^{202}Hg: −0.37‰, mean E^{199}Hg: −0.29‰). Aligning to a $\Delta^{199}Hg/\Delta^{201}Hg$ ratio of unity without discernible isotopic diel variations, Hg(0) effluxes overall appear to be governed by photochemical Hg(0) production in surface water. Our results indicate that water−atmosphere Hg(0) exchange overall could generate a positive shift of Δ^{199}Hg in fresh water, which provides an observational explanation for the positive odd-MIF signatures in present-day sediments.[80] Combining flux and isotope measurements with supplied ambient air and air with artificially high and low Hg(0) concentrations, the application of a mass balance model indicates that dry deposition of Hg(0) is of fundamental importance in atmospheric−water gas exchange. Results from the present study reveal that direct Hg(0) dry deposition fluxes greatly exceed the wet deposition fluxes at the investigated lakes, indicating a dominant role of Hg(0) dry deposition in the fresh water ecosystem, which is broadly consistent with pervious findings in lake sediments and marine ecosystems.[18,81,82]

Ocean Hg(0) emissions are an important source of atmospheric Hg,[15,16] yet the isotopic signatures of this emission source remain essentially unknown. In Figure S15, we draw an atmospheric Hg deposition mixing line based on the Δ^{199}Hg vs Δ^{200}Hg signatures of atmospheric Hg(0) and reactive Hg(II) and precipitation Hg(II). We found that Δ^{199}Hg of seawater DHg deviates positively (+0.07−0.11‰) from the atmospheric Hg deposition mixing line (Figure S15), similar to those of fresh water in our study (+0.03−0.26‰), which is attributed to water Hg(0) emissions, as discussed in Section 3.5. Furthermore, the contribution of atmospheric Hg(0) dry deposition to Hg in fresh water in our study is comparable to previously reported values of seawater.[18] We therefore postulate that odd-MIF of Hg isotopes during seawater Hg(0) emissions may resemble that of fresh water [i.e., negative odd-MIF in Hg(0) emissions], and this hypothesis could be also explained by the observations of negative Δ^{199}Hg values in Hg(0) in marine boundary layer air.[83,84] We caution that due to the insufficient knowledge of the gaseous oxidized mercury (GOM) isotopic signatures in the planetary boundary layer, such an interpretation may have large uncertainties. Previous studies observed much lower GOM Δ^{199}Hg values in arctic and marine boundary layer air as compared with the free troposphere.[85,86] An integration of these data would yield a lower Δ^{199}Hg of Hg delivered into waters and may further indicate a larger positive shift of Δ^{199}Hg during water Hg(0) emissions. Future in situ studies on the bidirectional exchange fluxes as well as their Hg isotope fractionation at the seawater and atmosphere interface are needed to better understand the roles of Hg(0) exchange in the cycling of Hg in the global atmosphere and oceans.

■ ASSOCIATED CONTENT

Supporting Information

The Supporting Information is available free of charge at https://pubs.acs.org/doi/10.1021/acs.est.3c01273.

Additional information of the study sites, experimental details, Hg isotopic mass balance model, concentrations, fluxes and isotopic compositions, and ancillary analysis of the data (PDF)

■ AUTHOR INFORMATION

Corresponding Author

Xuewu Fu − *State Key Laboratory of Environmental Geochemistry, Institute of Geochemistry, Chinese Academy of Sciences, Guiyang 550081, China;* orcid.org/0000-0002-5174-7150; Email: fuxuewu@mail.gyig.ac.cn

Authors

Hui Zhang − *State Key Laboratory of Environmental Geochemistry, Institute of Geochemistry, Chinese Academy of Sciences, Guiyang 550081, China; University of Chinese Academy of Sciences, Beijing 100049, China*

Xian Wu − *State Key Laboratory of Environmental Geochemistry, Institute of Geochemistry, Chinese Academy of Sciences, Guiyang 550081, China; University of Chinese Academy of Sciences, Beijing 100049, China*

Qianwen Deng − *State Key Laboratory of Environmental Geochemistry, Institute of Geochemistry, Chinese Academy of Sciences, Guiyang 550081, China; University of Chinese Academy of Sciences, Beijing 100049, China*

Kaihui Tang − *State Key Laboratory of Environmental Geochemistry, Institute of Geochemistry, Chinese Academy of Sciences, Guiyang 550081, China; University of Chinese Academy of Sciences, Beijing 100049, China*

Leiming Zhang − *Air Quality Research Division, Science and Technology Branch, Environment and Climate Change Canada, Toronto M3H5T4 Ontario, Canada;* orcid.org/0000-0001-5437-5412

Jonas Sommar − *State Key Laboratory of Environmental Geochemistry, Institute of Geochemistry, Chinese Academy of Sciences, Guiyang 550081, China*

Guangyi Sun − *State Key Laboratory of Environmental Geochemistry, Institute of Geochemistry, Chinese Academy of Sciences, Guiyang 550081, China;* orcid.org/0000-0001-8002-3576

Xinbin Feng − *State Key Laboratory of Environmental Geochemistry, Institute of Geochemistry, Chinese Academy of Sciences, Guiyang 550081, China; University of Chinese Academy of Sciences, Beijing 100049, China;* orcid.org/0000-0002-7462-8998

Complete contact information is available at:

https://doi.org/10.1021/acs.est.3c01273
Environ. Sci. Technol. 2023, 57, 10673−10685

https://pubs.acs.org/10.1021/acs.est.3c01273

Notes

The authors declare no competing financial interest.

■ ACKNOWLEDGMENTS

This work was funded by the Key Research Program of Frontier Science (ZDBS-LY-DQC029) and the Strategic Priority Research Program (XDB40020404), Chinese Academy of Sciences, the K.C. Wong Education Foundation, and the National Science Foundation of China (41921004).

■ REFERENCES

(1) Osterwalder, S.; Nerentorp, M.; Zhu, W.; Jiskra, M.; Nilsson, E.; Nilsson, M. B.; Rutgersson, A.; Soerensen, A. L.; Sommar, J.; Wallin, M. B.; Wängberg, I.; Bishop, K. Critical Observations of Gaseous Elemental Mercury Air-Sea Exchange. *Global Biogeochem. Cycles* **2021**, *35*, No. e2020GB006742.

(2) Sommar, J.; Osterwalder, S.; Zhu, W. Recent advances in understanding and measurement of Hg in the environment: Surface-atmosphere exchange of gaseous elemental mercury (Hg^0). *Sci. Total Environ.* **2020**, *721*, 137648.

(3) Tseng, C. M.; Lamborg, C. H.; Hsu, S. C. A unique seasonal pattern in dissolved elemental mercury in the South China Sea, a tropical and monsoon-dominated marginal sea. *Geophys. Res. Lett.* **2013**, *40*, 167−172.

(4) Lindberg, S.; Bullock, R.; Ebinghaus, R.; Engstrom, D.; Feng, X. B.; Fitzgerald, W.; Pirrone, N.; Prestbo, E.; Seigneur, C. A synthesis of progress and uncertainties in attributing the sources of mercury in deposition. *Ambio* **2007**, *36*, 19−33.

(5) Mason, R. P.; Sheu, G. R. Role of the ocean in the global mercury cycle. *Global Biogeochem. Cycles* **2002**, *16*, 40-1−40-14.

(6) Amyot, M.; Mierle, G.; Lean, D.; McQueen, D. J. Effect of solar radiation on the formation of dissolved gaseous mercury in temperate lakes. *Geochim. Cosmochim. Acta* **1997**, *61*, 975−987.

(7) Strode, S. A.; Jaegle, L.; Selin, N. E.; Jacob, D. J.; Park, R. J.; Yantosca, R. M.; Mason, R. P.; Slemr, F. Air-sea exchange in the global mercury cycle. *Global Biogeochem. Cycles* **2007**, *21*, GB1017.

(8) Fantozzi, L.; Ferrara, R.; Frontini, F. P.; Dini, F. Dissolved gaseous mercury production in the dark: Evidence for the fundamental role of bacteria in different types of Mediterranean water bodies. *Sci. Total Environ.* **2009**, *407*, 917−924.

(9) O'Driscoll, N. J.; Poissant, L.; Canario, J.; Lean, D. R. S. Dissolved gaseous mercury concentrations and mercury volatilization in a frozen freshwater fluvial lake. *Environ. Sci. Technol.* **2008**, *42*, 5125−5130.

(10) Zheng, W.; Liang, L. Y.; Gu, B. H. Mercury Reduction and Oxidation by Reduced Natural Organic Matter in Anoxic Environments. *Environ. Sci. Technol.* **2012**, *46*, 292−299.

(11) Ci, Z. J.; Zhang, X. S.; Yin, Y. G.; Chen, J. S.; Wang, S. W. Mercury Redox Chemistry in Waters of the Eastern Asian Seas: From Polluted Coast to Clean Open Ocean. *Environ. Sci. Technol.* **2016**, *50*, 2371−2380.

(12) Soerensen, A. L.; Sunderland, E. M.; Holmes, C. D.; Jacob, D. J.; Yantosca, R. M.; Skov, H.; Christensen, J. H.; Strode, S. A.; Mason, R. P. An Improved Global Model for Air-Sea Exchange of Mercury: High Concentrations over the North Atlantic. *Environ. Sci. Technol.* **2010**, *44*, 8574−8580.

(13) Zheng, W.; Demers, J. D.; Lu, X.; Bergquist, B. A.; Anbar, A. D.; Blum, J. D.; Gu, B. H. Mercury Stable Isotope Fractionation during Abiotic Dark Oxidation in the Presence of Thiols and Natural Organic Matter. *Environ. Sci. Technol.* **2019**, *53*, 1853−1862.

(14) Garcia, E.; Poulain, A. J.; Amyot, M.; Ariya, P. A. Diel variations in photoinduced oxidation of Hg-0 in freshwater. *Chemosphere* **2005**, *59*, 977−981.

(15) Selin, N. E. Global Biogeochemical Cycling of Mercury: A Review. *Annu. Rev. Environ. Resour.* **2009**, *34*, 43−63.

(16) Horowitz, H. M.; Jacob, D. J.; Zhang, Y. X.; Dibble, T. S.; Slemr, F.; Amos, H. M.; Schmidt, J. A.; Corbitt, E. S.; Marais, E. A.; Sunderland, E. M. A new mechanism for atmospheric mercury redox chemistry: implications for the global mercury budget. *Atmos. Chem. Phys.* **2017**, *17*, 6353−6371.

(17) Yuan, W.; Wang, X.; Lin, C. J.; Sommar, J. O.; Wang, B.; Lu, Z. Y.; Feng, X. B. Quantification of Atmospheric Mercury Deposition to and Legacy Re-emission from a Subtropical Forest Floor by Mercury Isotopes. *Environ. Sci. Technol.* **2021**, *55*, 12352−12361.

(18) Jiskra, M.; Heimburger-Boavida, L. E.; Desgranges, M. M.; Petrova, M. V.; Dufour, A.; Ferreira-Araujo, B.; Masbou, J.; Chmeleff, J.; Thyssen, M.; Point, D.; Sonke, J. E. Mercury stable isotopes constrain atmospheric sources to the ocean. *Nature* **2021**, *597*, 678−682.

(19) Jiskra, M.; Wiederhold, J. G.; Skyllberg, U.; Kronberg, R. M.; Hajdas, I.; Kretzschmar, R. Mercury Deposition and Re-emission Pathways in Boreal Forest Soils Investigated with Hg Isotope Signatures. *Environ. Sci. Technol.* **2015**, *49*, 7188−7196.

(20) Kritee, K.; Blum, J. D.; Reinfelder, J. R.; Barkay, T. Microbial stable isotope fractionation of mercury: A synthesis of present understanding and future directions. *Chem. Geol.* **2013**, *336*, 13−25.

(21) Bergquist, B. A.; Blum, J. D. Mass-dependent and -independent fractionation of Hg isotopes by photoreduction in aquatic systems. *Science* **2007**, *318*, 417−420.

(22) Koster van Groos, P. G.; Esser, B. K.; Williams, R. W.; Hunt, J. R. Isotope Effect of Mercury Diffusion in Air. *Environ. Sci. Technol.* **2014**, *48*, 227−233.

(23) Blum, J. D.; Popp, B. N.; Drazen, J. C.; Anela Choy, C.; Johnson, M. W. Methylmercury production below the mixed layer in the North Pacific Ocean. *Nat. Geosci.* **2013**, *6*, 879−884.

(24) Ghosh, S.; Schauble, E. A.; Lacrampe Couloume, G.; Blum, J. D.; Bergquist, B. A. Estimation of nuclear volume dependent fractionation of mercury isotopes in equilibrium liquid-vapor evaporation experiments. *Chem. Geol.* **2013**, *336*, 5−12.

(25) Estrade, N.; Carignan, J.; Sonke, J. E.; Donard, O. F. X. Mercury isotope fractionation during liquid-vapor evaporation experiments. *Geochim. Cosmochim. Acta* **2009**, *73*, 2693−2711.

(26) Zheng, W.; Hintelmann, H. Nuclear Field Shift Effect in Isotope Fractionation of Mercury during Abiotic Reduction in the Absence of Light. *J. Phys. Chem. A* **2010**, *114*, 4238−4245.

(27) Motta, L. C.; Kritee, K.; Blum, J. D.; Tsz-Ki Tsui, M.; Reinfelder, J. R. Mercury Isotope Fractionation during the Photochemical Reduction of Hg(II) Coordinated with Organic Ligands. *J. Phys. Chem. A* **2020**, *124*, 2842−2853.

(28) Motta, L. C.; Chien, A. D.; Rask, A. E.; Zimmerman, P. M. Mercury Magnetic Isotope Effect: A Plausible Photochemical Mechanism. *J. Phys. Chem. A* **2020**, *124*, 3711−3719.

(29) Wiederhold, J. G. Metal Stable Isotope Signatures as Tracers in Environmental Geochemistry. *Environ. Sci. Technol.* **2015**, *49*, 2606−2624.

(30) Zheng, W.; Hintelmann, H. Isotope Fractionation of Mercury during Its Photochemical Reduction by Low-Molecular-Weight Organic Compounds. *J. Phys. Chem. A* **2010**, *114*, 4246−4253.

(31) Zheng, W.; Foucher, D.; Hintelmann, H. Mercury isotope fractionation during volatilization of Hg(0) from solution into the gas phase. *J. Anal. At. Spectrom.* **2007**, *22*, 1097−1104.

(32) Kritee, K.; Blum, J. D.; Barkay, T. Mercury Stable Isotope Fractionation during Reduction of Hg(II) by Different Microbial Pathways. *Environ. Sci. Technol.* **2008**, *42*, 9171−9177.

(33) Fu, X. W.; Jiskra, M.; Yang, X.; Marusczak, N.; Enrico, M.; Chmeleff, J.; Heimburger-Boavida, L. E.; Gheusi, F.; Sonke, J. E. Mass-Independent Fractionation of Even and Odd Mercury Isotopes during Atmospheric Mercury Redox Reactions. *Environ. Sci. Technol.* **2021**, *55*, 10164−10174.

(34) Chen, J. B.; Hintelmann, H.; Feng, X. B.; Dimock, B. Unusual fractionation of both odd and even mercury isotopes in precipitation from Peterborough, ON, Canada. *Geochim. Cosmochim. Acta* **2012**, *90*, 33−46.

(35) Sun, G. Y.; Feng, X. B.; Yin, R. S.; Wang, F. Y.; Lin, C. J.; Li, K.; Sommar, J. O. Dissociation of Mercuric Oxides Drives Anomalous Isotope Fractionation during Net Photo-oxidation of Mercury Vapor in Air. *Environ. Sci. Technol.* **2022**, *56*, 13428−13438.
(36) Wang, B.; Chen, M.; Ding, L.; Zhao, Y. H.; Man, Y.; Feng, L.; Li, P.; Zhang, L. M.; Feng, X. B. Fish, rice, and human hair mercury concentrations and health risks in typical Hg-contaminated areas and fish-rich areas, China. *Environ. Int.* **2021**, *154*, 106561.
(37) Yuan, W.; Sommar, J.; Lin, C. J.; Wang, X.; Li, K.; Liu, Y.; Zhang, H.; Lu, Z. Y.; Wu, C. S.; Feng, X. B. Stable Isotope Evidence Shows Re-emission of Elemental Mercury Vapor Occurring after Reductive Loss from Foliage. *Environ. Sci. Technol.* **2019**, *53*, 651−660.
(38) Zhu, W.; Fu, X. W.; Zhang, H.; Liu, C.; Skyllberg, U.; Sommar, J.; Yu, B.; Feng, X. B. Mercury Isotope Fractionation during the Exchange of Hg(0) between the Atmosphere and Land Surfaces: Implications for Hg(0) Exchange Processes and Controls. *Environ. Sci. Technol.* **2022**, *56*, 1445−1457.
(39) Demers, J. D.; Blum, J. D.; Zak, D. R. Mercury isotopes in a forested ecosystem: Implications for air-surface exchange dynamics and the global mercury cycle. *Global Biogeochem. Cycles* **2013**, *27*, 222−238.
(40) Zhang, H.; Tan, Q. Y.; Zhang, L. M.; Fu, X. W.; Feng, X. B. A Laboratory Study on the Isotopic Composition of Hg(0) Emitted From Hg-Enriched Soils in Wanshan Hg Mining Area. *J. Geophys. Res. Atmos.* **2020**, *125*, No. e2020JD032572.
(41) Zhao, H.; Meng, B.; Sun, G.; Lin, C.-J.; Feng, X.; Sommar, J. Chemistry and Isotope Fractionation of Divalent Mercury during Aqueous Reduction Mediated by Selected Oxygenated Organic Ligands. *Environ. Sci. Technol.* **2021**, *55*, 13376−13386.
(42) Sun, R. Y.; Jiskra, M.; Amos, H. M.; Zhang, Y. X.; Sunderland, E. M.; Sonke, J. E. Modelling the mercury stable isotope distribution of Earth surface reservoirs: Implications for global Hg cycling. *Geochim. Cosmochim. Acta* **2019**, *246*, 156−173.
(43) Sonke, J. E. A global model of mass independent mercury stable isotope fractionation. *Geochim. Cosmochim. Acta* **2011**, *75*, 4577−4590.
(44) Fu, X. W.; Feng, X. B.; Guo, Y. N.; Meng, B.; Yin, R. S.; Yao, H. Distribution and production of reactive mercury and dissolved gaseous mercury in surface waters and water/air mercury flux in reservoirs on Wujiang River, Southwest China. *J. Geophys. Res. Atmos.* **2013**, *118*, 3905−3917.
(45) Fu, X. W.; Heimburger, L. E.; Sonke, J. E. Collection of atmospheric gaseous mercury for stable isotope analysis using iodine- and chlorine-impregnated activated carbon traps. *J Anal Atom Spectrom* **2014**, *29*, 841−852.
(46) Zhang, H.; Wu, X.; Deng, Q. W.; Zhang, L. M.; Fu, X. W.; Feng, X. B. Extraction of ultratrace dissolved gaseous mercury and reactive mercury in natural freshwater for stable isotope analysis. *J Anal Atom Spectrom* **2021**, *36*, 1921−1932.
(47) EPA, U. *Method 1631, Revision E:, Mercury in Water by Oxidation, Purge and Trap, and Cold Vapor Atomic Fluorescence Spectrometry (EPA, 2002)*; United States Environmental Protection Agency: Washington, DC, 2002, pp 1−33.
(48) Yu, B.; Fu, X. W.; Yin, R. S.; Zhang, H.; Wang, X.; Lin, C. J.; Wu, C. S.; Zhang, Y. P.; He, N. N.; Fu, P. Q.; Wang, Z. F.; Shang, L. H.; Sommar, J.; Sonke, J. E.; Maurice, L.; Guinot, B.; Feng, X. B. Isotopic Composition of Atmospheric Mercury in China: New Evidence for Sources and Transformation Processes in Air and in Vegetation. *Environ. Sci. Technol.* **2016**, *50*, 9262−9269.
(49) Yin, R. S.; Feng, X. B.; Foucher, D.; Shi, W. F.; Zhao, Z. Q.; Wang, J. High Precision Determination of Mercury Isotope Ratios Using Online Mercury Vapor Generation System Coupled with Multicollector Inductively Coupled Plasma-Mass Spectrometer. *Chin. J. Anal. Chem.* **2010**, *38*, 929−934.
(50) Blum, J. D.; Bergquist, B. A. Reporting of variations in the natural isotopic composition of mercury. *Anal. Bioanal. Chem.* **2007**, *388*, 353−359.
(51) Blum, J. D.; Johnson, M. W. Recent Developments in Mercury Stable Isotope Analysis. *Rev. Mineral. Geochem.* **2017**, *82*, 733−757.
(52) Estrade, N.; Carignan, J.; Sonke, J. E.; Donard, O. F. X. Measuring Hg Isotopes in Bio-Geo-Environmental Reference Materials. *Geostand. Geoanal. Res.* **2010**, *34*, 79−93.
(53) Chen, J. B.; Hintelmann, H.; Zheng, W.; Feng, X. B.; Cai, H. M.; Wang, Z. H.; Yuan, S. L.; Wang, Z. W. Isotopic evidence for distinct sources of mercury in lake waters and sediments. *Chem. Geol.* **2016**, *426*, 33−44.
(54) Sprovieri, F.; Pirrone, N.; Bencardino, M.; D'Amore, F.; Carbone, F.; Cinnirella, S.; Mannarino, V.; Landis, M.; Ebinghaus, R.; Weigelt, A.; Brunke, E. G.; Labuschagne, C.; Martin, L.; Munthe, J.; Wangberg, I.; Artaxo, P.; Morais, F.; Barbosa, H. d. M. J.; Brito, J.; Cairns, W.; Barbante, C.; Dieguez, M. D.; Garcia, P. E.; Dommergue, A.; Angot, H.; Magand, O.; Skov, H.; Horvat, M.; Kotnik, J.; Read, K. A.; Neves, L. M.; Gawlik, B. M.; Sena, F.; Mashyanov, N.; Obolkin, V.; Wip, D.; Feng, X. B.; Zhang, H.; Fu, X. W.; Ramachandran, R.; Cossa, D.; Knoery, J.; Marusczak, N.; Nerentorp, M.; Norstrom, C. Atmospheric mercury concentrations observed at ground-based monitoring sites globally distributed in the framework of the GMOS network. *Atmos. Chem. Phys.* **2016**, *16*, 11915−11935.
(55) Kwon, S. Y.; Blum, J. D.; Yin, R.; Tsui, M. T. K.; Yang, Y. H.; Choi, J. W. Mercury stable isotopes for monitoring the effectiveness of the Minamata Convention on Mercury. *Earth-Sci. Rev.* **2020**, *203*, 103111.
(56) Fu, X. W.; Liu, C.; Zhang, H.; Xu, Y.; Zhang, H.; Li, J.; Lyu, X.; Zhang, G.; Guo, H.; Wang, X.; Zhang, L.; et al. Isotopic compositions of atmospheric total gaseous mercury in 10 Chinese cities and implications for land surface emissions. *Atmos. Chem. Phys.* **2021**, *21*, 6721−6734.
(57) Ci, Z. J.; Zhang, X. S.; Wang, Z. W. Elemental mercury in coastal seawater of Yellow Sea, China: Temporal variation and air-sea exchange. *Atmos. Environ.* **2011**, *45*, 183−190.
(58) Fantozzi, L.; Manca, G.; Ammoscato, I.; Pirrone, N.; Sprovieri, F. The cycling and sea-air exchange of mercury in the waters of the Eastern Mediterranean during the 2010 MED-OCEANOR cruise campaign. *Sci. Total Environ.* **2013**, *448*, 151−162.
(59) Andersson, M. E.; Sommar, J.; Gardfeldt, K.; Lindqvist, O. Enhanced concentrations of dissolved gaseous mercury in the surface waters of the Arctic Ocean. *Mar. Chem.* **2008**, *110*, 190−194.
(60) Amyot, M.; Gill, G. A.; Morel, F. M. M. Production and loss of dissolved gaseous mercury in coastal seawater. *Environ. Sci. Technol.* **1997**, *31*, 3606−3611.
(61) Lalonde, J. D.; Amyot, M.; Orvoine, J.; Morel, F. M. M.; Auclair, J. C.; Ariya, P. A. Photoinduced oxidation of Hg-0 (aq) in the waters from the St. Lawrence estuary. *Environ. Sci. Technol.* **2004**, *38*, 508−514.
(62) Jiskra, M.; Sonke, J. E.; Agnan, Y.; Helmig, D.; Obrist, D. Insights from mercury stable isotopes on terrestrial-atmosphere exchange of Hg(0) in the Arctic tundra. *Biogeosciences* **2019**, *16*, 4051−4064.
(63) Stathopoulos, D. Fractionation of Mercury Isotopes in an Aqueous Environment: Chemical Oxidation. M.Sc. Thesis, TrentUniversity, Peterborough, Canada, 2014.
(64) Sun, G. Y.; Sommar, J.; Feng, X. B.; Lin, C. J.; Ge, M. F.; Wang, W. G.; Yin, R. S.; Fu, X. W.; Shang, L. H. Mass-Dependent and -Independent Fractionation of Mercury Isotope during Gas-Phase Oxidation of Elemental Mercury Vapor by Atomic Cl and Br. *Environ. Sci. Technol.* **2016**, *50*, 9232−9241.
(65) Shah, V.; Jacob, D. J.; Thackray, C. P.; Wang, X.; Sunderland, E. M.; Dibble, T. S.; Saiz-Lopez, A.; Cernusak, I.; Kello, V.; Castro, P. J.; Wu, R. R.; Wang, C. J. Improved Mechanistic Model of the Atmospheric Redox Chemistry of Mercury. *Environ. Sci. Technol.* **2021**, *55*, 14445−14456.
(66) Lindberg, S. E.; Vette, A. F.; Miles, C.; Schaedlich, F. Mercury speciation in natural waters: Measurement of dissolved gaseous mercury with a field analyzer. *Biogeochemistry* **2000**, *48*, 237−259.

(67) Zheng, W.; Hintelmann, H. Mercury isotope fractionation during photoreduction in natural water is controlled by its Hg/DOC ratio. *Geochim. Cosmochim. Acta* **2009**, *73*, 6704−6715.
(68) Gustin, M. S.; Ericksen, J. A.; Schorran, D. E.; Johnson, D. W.; Lindberg, S. E.; Coleman, J. S. Application of controlled mesocosms for understanding mercury air-soil-plant exchange. *Environ. Sci. Technol.* **2004**, *38*, 6044−6050.
(69) Sherman, L. S.; Blum, J. D.; Johnson, K. P.; Keeler, G. J.; Barres, J. A.; Douglas, T. A. Mass-independent fractionation of mercury isotopes in Arctic snow driven by sunlight. *Nat Geosci* **2010**, *3*, 173−177.
(70) Haitzer, M.; Aiken, G. R.; Ryan, J. N. Binding of mercury(II) to dissolved organic matter: The role of the mercury-to-DOM concentration ratio. *Environ. Sci. Technol.* **2002**, *36*, 3564−3570.
(71) Hesterberg, D.; Chou, J. W.; Hutchison, K. J.; Sayers, D. E. Bonding of Hg(II) to reduced organic, sulfur in humic acid as affected by S/Hg ratio. *Environ. Sci. Technol.* **2001**, *35*, 2741−2745.
(72) Jiang, T.; Skyllberg, U.; Wei, S. Q.; Wang, D. Y.; Lu, S.; Jiang, Z. M.; Flanagan, D. C. Modeling of the structure-specific kinetics of abiotic, dark reduction of Hg(II) complexed by O/N and S functional groups in humic acids while accounting for time-dependent structural rearrangement. *Geochim. Cosmochim. Acta* **2015**, *154*, 151−167.
(73) Wiederhold, J. G.; Cramer, C. J.; Daniel, K.; Infante, I.; Bourdon, B.; Kretzschmar, R. Equilibrium Mercury Isotope Fractionation between Dissolved Hg(II) Species and Thiol-Bound Hg. *Environ. Sci. Technol.* **2010**, *44*, 4191−4197.
(74) He, T. R. Biogeochemical cycling of mercury in Hongfeng Reservior, Guizhou,China. D, Sc, Thesis, University of Chinese Academy of Science, China, 2007.
(75) Zeng, Y.; Chen, J. G.; Yang, Y. Q.; Wang, J. X.; Zhu, Z. J.; Li, J. Huguangyan Maar Lake (SE China): A solid record of atmospheric mercury pollution history in a non-remote region. *J. Asian Earth Sci.* **2017**, *147*, 1−8.
(76) Yin, R. S.; Feng, X. B.; Hurley, J. P.; Krabbenhoft, D. P.; Lepak, R. F.; Kang, S. C.; Yang, H. D.; Li, X. D. Historical Records of Mercury Stable Isotopes in Sediments of Tibetan Lakes. *Sci. Rep.* **2016**, *6*, 23332.
(77) Fu, X. W.; Zhu, W.; Zhang, H.; Sommar, J.; Yu, B.; Yang, X.; Wang, X.; Lin, C. J.; Feng, X. B. Depletion of atmospheric gaseous elemental mercury by plant uptake at Mt. Changbai, Northeast China. *Atmos. Chem. Phys.* **2016**, *16*, 12861−12873.
(78) Obrist, D.; Roy, E. M.; Harrison, J. L.; Kwong, C. F.; Munger, J. W.; Moosmuller, H.; Romero, C. D.; Sun, S. W.; Zhou, J.; Commane, R. Previously unaccounted atmospheric mercury deposition in a midlatitude deciduous forest. *Proc. Natl. Acad. Sci. U.S.A.* **2021**, *118*, No. e2105477118.
(79) Feng, X. B.; Li, P.; Fu, X. W.; Wang, X.; Zhang, H.; Lin, C. J. Mercury pollution in China: implications on the implementation of the Minamata Convention. *Environ. Sci.: Processes Impacts* **2022**, *24*, 634−648.
(80) Lee, J. H.; Kwon, S. Y.; Yin, R. S.; Motta, L. C.; Kurz, A. Y.; Nam, S. I. Spatiotemporal Characterization of Mercury Isotope Baselines and Anthropogenic Influences in Lake Sediment Cores. *Global Biogeochem. Cycles* **2021**, *35*, No. e2020GB006904.
(81) Enrico, M.; Roux, G. L.; Marusczak, N.; Heimburger, L. E.; Claustres, A.; Fu, X. W.; Sun, R. Y.; Sonke, J. E. Atmospheric Mercury Transfer to Peat Bogs Dominated by Gaseous Elemental Mercury Dry Deposition. *Environ. Sci. Technol.* **2016**, *50*, 2405−2412.
(82) Woerndle, G. E.; Tsz-Ki Tsui, M.; Sebestyen, S. D.; Blum, J. D.; Nie, X. P.; Kolka, R. K. New Insights on Ecosystem Mercury Cycling Revealed by Stable Isotopes of Mercury in Water Flowing from a Headwater Peatland Catchment. *Environ. Sci. Technol.* **2018**, *52*, 1854−1861.
(83) Fu, X. W.; Yang, X.; Tan, Q. Y.; Ming, L. L.; Lin, T.; Lin, C. J.; Li, X. D.; Feng, X. B. Isotopic Composition of Gaseous Elemental Mercury in the Boundary Layer Of East China Sea. *J. Geophys. Res. Atmos.* **2018**, *123*, 7656−7669.
(84) Demers, J. D.; Sherman, L. S.; Blum, J. D.; Marsik, F. J.; Dvonch, J. T. Coupling atmospheric mercury isotope ratios and meteorology to identify sources of mercury impacting a coastal urban-industrial region near Pensacola, Florida, USA. *Global Biogeochem. Cycles* **2015**, *29*, 1689−1705.
(85) Rolison, J. M.; Landing, W. M.; Luke, W.; Cohen, M.; Salters, V. J. M. Isotopic composition of species-specific atmospheric Hg in a coastal environment. *Chem. Geol.* **2013**, *336*, 37−49.
(86) Araujo, B. F.; Osterwalder, S.; Szponar, N.; Lee, D.; Petrova, M. V.; Pernov, J. B.; Ahmed, S.; Heimburger-Boavida, L. E.; Laffont, L.; Teisserenc, R.; Tananaev, N.; Nordstrom, C.; Magand, O.; Stupple, G.; Skov, H.; Steffen, A.; Bergquist, B.; Pfaffhuber, K. A.; Thomas, J. L.; Scheper, S.; Petaja, T.; Dommergue, A.; Sonke, J. E. Mercury isotope evidence for Arctic summertime re-emission of mercury from the cryosphere. *Nat. Commun.* **2022**, *13*, 4956.

https://doi.org/10.1021/acs.est.3c01273
Environ. Sci. Technol. 2023, 57, 10673−10685